UNIVERSITY OF CALIFORNIA, SAN DIEGO

A Self-assembling RNA Nanoprism

A Thesis submitted in partial satisfaction of the requirements
for the degree Master of Science

in

Materials Science and Engineering

by

Shi Chen

Committee in Charge:

Professor Thomas Hermann, Chair
Professor Adah Almutairi
Professor Michael K. Gilson
Professor Jerry Yang

2016

The thesis of Shi Chen is approved, and it is acceptable in quality and form for publication on microfilm and electronically:

_____

_____

_____

_____

Chair

University of San Diego

2016

Dedication

I dedicate this thesis to my father, Donglin Chen

and my mother, Lan Sun

and my girlfriend, Jingrong Yan

Table of Contents

List of Abbreviations

RNA: Ribonucleic Acid

DNA: Deoxyribonucleic Acid

mRNA: messenger RNA

rRNA: ribosomal RNA

tRNA: transfer RNA

ΔG: Gibbs Free Energy

SVV: Seneca Valley Virus

HCV: Hepatitis C Virus

IRES: Internal Ribosome Entry Sites

PAGE: Polyacrylamide Gel Electrophoresis

APS: Ammonium Persulfate

TEMED: Tetramethylethylenediamine

EMF: Electromotive Force

FRET: Förster Resonance Energy Transfer

E: Efficiency of Energy Transfer in FRET

R_0: Förster Distance

AFM: Atomic Force Microscopy

SEM: Scanning Electronic Microscopy

TEM: Transmission electronic microscopy

ssRNA: Single-stranded RNA

List of Figures

List of Tables

Acknowledgements

Firstly, I want to thank Prof. Thomas Hermann who guided me to complete this project. He gave me so much patience when things went wrong and so much valuable advice when I had no idea about what to do next. He is the best professor I have ever met.

Secondly, I want to thank all my lab mates who helped me finish this project. I want to especially thank Mark Boerneke, a fifth-year PhD in my lab, who taught me all the techniques I used in this thesis.

Thirdly, I would like to thank my parents, Donglin Chen (father) and Lan Sun (mother), for supporting me financially and mentally during my master's in University of California, San Diego.

Abstract of the Thesis

A Self-assembling RNA Nanoprism

by

Shi Chen

Master of Science in Materials Science and Engineering

University of California, San Diego, 2016

Professor Thomas Hermann, Chair

Increasing attention has been paid into RNA as a building block to make nanostructures in the past two decades. The goal of this study was to make a nanoprism which was fully made of double-stranded RNA by an efficient self-assembly method. This was done by extending a nanotriangle which was rationally designed and made from an RNA conformational switch in the internal ribosome entry site (IRES) of Seneca Valley virus (SVV) and then combining two extended triangles with DNA or RNA splints. The successful extension and

combination of triangles were investigated by native polyacrylamide gel electrophoresis (PAGE). Details of the structure were further analyzed by Förster resonance energy transfer (FRET) methods, fluorescence quenching methods, and atomic force microscopy (AFM).

Chapter 1. Introduction

1.1 RNA and RNA Structure

Ribonucleic acid (RNA), which is a polymeric material playing a key role in origins of life, has multiple functions. A well-known example is the essential role of RNA in the central dogma in which deoxyribonucleic acid (DNA) is transcribed to mRNA which is then translated to protein (1). Those multiple functions are determined by both the sequence and structure of RNA. Therefore, in order to understand how RNA works, an in-depth knowledge of RNA structure is required.

RNA is a linear macromolecule which consists of monomers named nucleotides. One nucleotide is made up of one of four nitrogenous bases, a ribose sugar with 5 carbons numbered from 1’ to 5’, and a phosphate residue. As shown in Figure 1.1, the nitrogenous base is covalently bonded to 1’ position, while one phosphate residue is bonded to 3’ position of one sugar group and 5’ position of another sugar group by covalent bonds either.

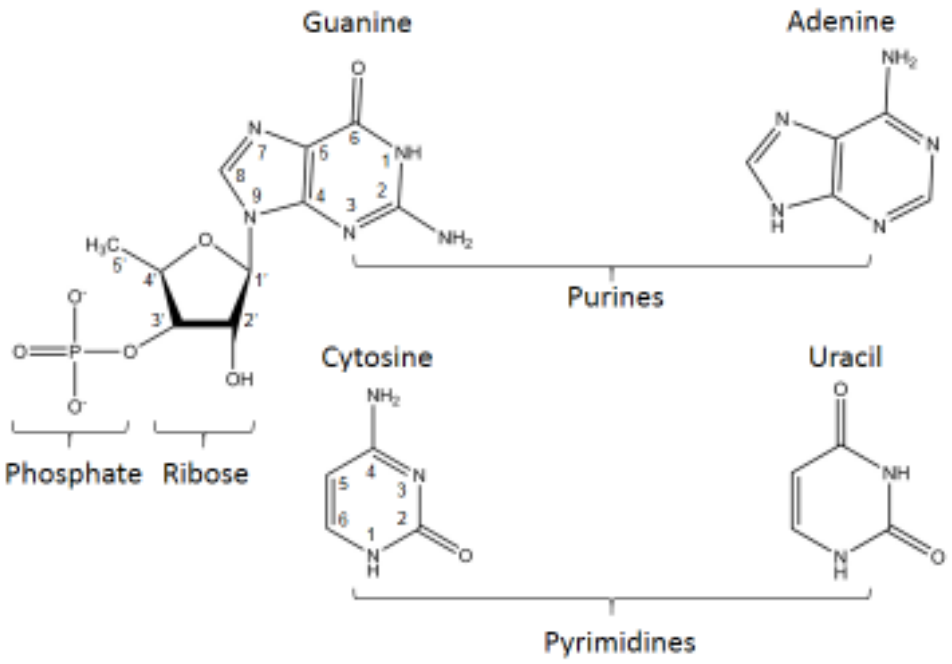

Figure 1.1 Building block of RNA

Four different nitrogenous groups (as shown in Figure 1.1) are divided into two types: purines, including adenine (A) and guanine (G), and pyrimidines, including cytosine (C) and uracil (U). The covalent bond connects the 1’ carbon of the ribose with the 9 nitrogen from a purine base or with the 1 nitrogen from a pyrimidine base.

Unlike DNA, which folds into double strands naturally, RNA is typically found in nature as a single-stranded chain. RNA molecules can fold upon themselves by base pairing or by interacting with another RNA chain to form a double helix by hydrogen bonds between adenine and uracil, as well as guanine and cytosine. The A-form double helix, instead of the B-form which commonly presents in DNA double helix, is favored by RNA double strands because of the

hydroxyl group at the 2’ carbon of sugar base in RNA. The A-form double helix, which has 11 base pairs in one turn of 2.8nm and 2.3nm in diameter, is shorter and wider than the B-form double helix which rises 3.4nm in each turn and exhibits 1.9nm in diameter (2, 3).

The structure of RNA is usually described from three levels. The primary structure is the linear sequences of nucleotides (AUGC), which are presented from the 5’ to 3’ end. The secondary structure relying on the Watson-Crick base pairing occurs when a RNA chain folds upon itself. Common elements in the secondary structure include hairpins, bulges and internal loops. The tertiary structure refers to the precise three-dimensional structure of RNA, which determines diverse functions of RNA.

The length of RNA in nature varies. The shortest RNA that has already been found only contains 22 nucleotides (4), while a long RNA chain can be able to contain as many as 17000 nucleotides (5). The variety in number of nucleotides, along with four different nitrogenous groups, results in the diversity of RNA.

A common way to classify RNAs is according to function. For example, in terms of RNAs involved in protein synthesis, RNAs are classified into messenger RNA (mRNA), ribosomal RNA (rRNA), transfer RNA (tRNA), etc. Some common RNAs in nature are listed in Table 1.

Table 1. Some common RNAs in nature classified according to function

RNA Involves in Protein Synthesis	Regulatory RNA	RNAs Involved in Post-Tanscriptional Modification
Message RNA	Antisense RNA	Guide RNA
Ribosomal RNA	CRISPR RNA	Ribonuclease MRP
Transfer RNA	Long noncoding RNA	Ribonuclease P
Transfer-messenger RNA	Trans-acting siRNA	Small nuclear RNA
	MicroRNA	Small nucleolar RNA
	Repeat associated siRNA	
	Small interfering RNA	

1.2 RNA Nanotechnology

RNA as a key part in forms of life has long been recognized (6), while its polymeric nature in materials has been underappreciated for a long time. Recently, however, it has been recognized that RNA, a seemingly unstable polymer material, can be used as a building block in applications of materials science.

1.2.1 RNA, a special polymer material

Polymers, which consist of large molecules composed of numerous repeating units named monomers, have been widely applied in materials science owing to outstanding properties, such as light weight, elasticity, etc. (7–9). Those special properties are mainly determined by the monomers and microstructures,

such as chain length and polymer architecture (linear and branched). Chain length, also referring to average molecular weight, determines mechanical properties of a polymer, while polymer architecture plays a dominant role in elasticity and thermal stability. Besides, given the types of monomer, polymers are divided into homopolymers which are polymerized by only one type of monomer and heteropolymers which contain two or even more different types of monomers.

RNA, which contains nucleotides as repeating units, can also be regarded as a polymer material. But since four different nucleotides are the monomer units of RNA, a special homogeneity is required to describe RNA. More specifically, RNA is a homopolymer made from nucleotides, but also a heteropolymer with regard to the four different building blocks A, U, G, and C (10). In terms of thermal stability, single-stranded RNA is capable to retain its native structure at low temperature, while high temperature leads to dissociation or misfolding, which compares to thermoplastic properties of synthetic polymers.

Synthetic polymers which are usually made through chain-growth polymerization and condensation polymerization usually have high polydispersity. RNA chains, however, are synthesized by enzymatic, template-dependent transcription which is similar to a condensation reaction, giving RNA chains defined sequence, specific structure and a polydispersity of index of 1. This high consistence in molecular weight is of great importance in practical applications because high polydispersity in polymers weakens mechanical

properties of materials. The defined length and structure of RNA chains also proved advantageous to applications in designing and building RNA nanostructures (11, 12).

1.2.2 Advantages compared to DNA as building blocks

DNA as a potential building block in materials science has been widely explored (13–15), and an exciting breakthrough came from introduction of a ‘scaffold’ for the assembly of complex periodic structures (16).

Compared with DNA, RNA as a building block has some distinct attributes. First of all, among hybrids of DNA-DNA, DNA-RNA and RNA-RNA, double-stranded RNA provides the thermodynamically most stable helix (17, 18). Another remarkable attribute of RNA is that RNA nanoparticles have a high propensity to self-assemble in vivo. By introducing DNA templates that code for RNA transcripts as building blocks, small RNA particles can be produced in cells. For example, a kissing loop formed between a synthesized RNA hairpin and a loop in trans-activation response (TAR) element has been found to possibly occur in a virus life circle (19).

1.2.3 Self-assembly tactic for the construction of RNA nanostructures

Self-assembly is a promising bottom-up approach that utilizes Watson-Crick base pairs and intrinsically defined features of RNA to build RNA nanostructures. This prominent approach is divided into two categories: templated and non-templated assembly (20). Templated assembly prepares

RNA chains by interacting components with another template under the influence of external force or structure, while non-templated assembly step-wisely grows RNA chain without introducing external template and forces. The examples for the former category include RNA transcription, hybridization, etc., while rational design and assembly of RNA nanostructures are in the realm of the later one.

1.2.4 Achievements in the field of RNA nanotechnology

The concept of RNA nanotechnology became well-known about two decades ago when Peixuan Guo and colleagues reported a pRNA ring that self-assembled from six identical RNA modules (21). In 2004, Luc Jaeger and colleagues made use of kissing-loop interactions between RNA modules termed “tectoRNA” to build an RNA nanosquare, in which four tectoRNAs were combined by four distinct, non-covalent loop-loop interactions (11). These previous studies laid the foundation to generate programmable nanostructures from small RNA motifs by self-assembly. As the value of RNA nanotechnology in practical applications has been recognized in many fields, such as targeted therapeutic delivery (22, 23), tissue engineering (24), etc., greater attention has been paid to RNA nanotechnology, and diverse structures have been designed and built. Our lab reported an RNA nanotriangle (Figure 1.2A) and nanosquare (Figure 1.2B) which were made of short oligonucleotides derived from RNA switches in the internal ribosome entry site (IRES) of Seneca Valley virus (SVV) and hepatitis C virus (HCV), respectively (25, 26). X-ray crystallography was used to demonstrate that these nanoarchitectures represent the smallest

possible triangle and square structure made from double-stranded RNA. The concept of this work exploiting efficient self-assembly of short oligonucleotides paved a way to build small RNA nanoobjects. Guo and coworkers introduced a conceptual approach to the rational design of three different RNA architectures (triangle, square and pentagon, as shown in Figure 1.2c) from a pRNA three-way junction (3WJ) motif by stretching the RNA motif to different conformations (60º, 90º and 108º) (27). This work amazingly built different nanoparticles from the same RNA building motif, making it a promising design for medical applications where multiple nano-vehicles are required to be built from a single building block.

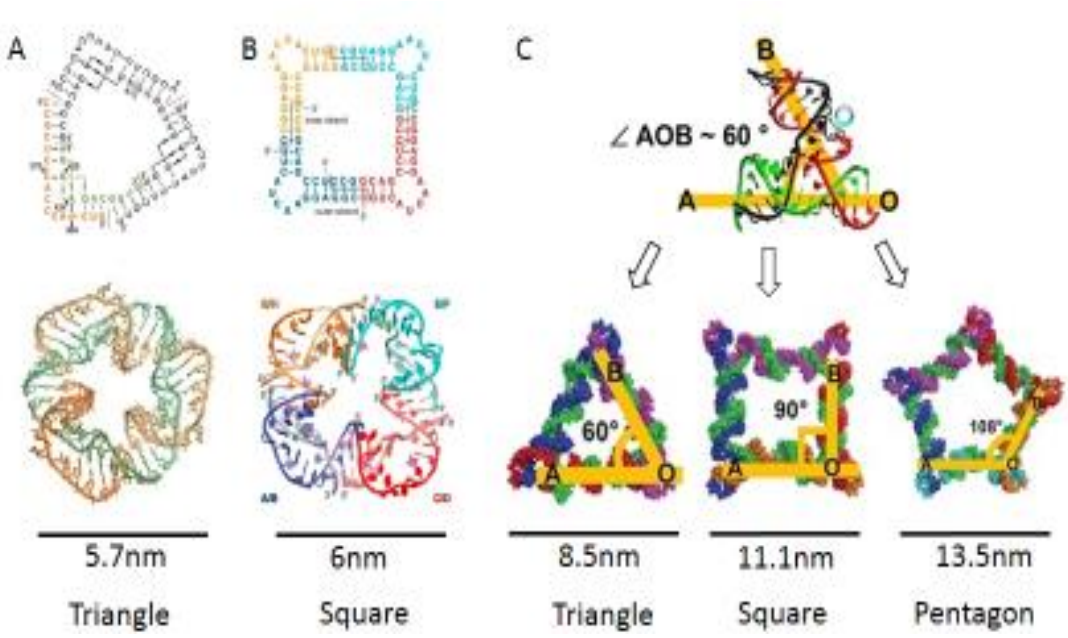

Figure 1.2 Two-dimensional RNA nanostructures. (A) Nanotriangle made from SVV IIa domains from the ref. (25). (B) Nanosquare made from HCV IIa domains from the ref. (26). (C) Triangle, square, pentagon made from pRNA 3WJ motif from the ref. (27).

Beyond such two-dimensional nanostructures, efforts have been made to obtain three-dimensional RNA nanostructures with more elaborate design. A

polyhedron (Figure 1.3A) made of tRNA was reported by Jaeger and colleagues for the first time (28). This 3D structure could be made by either an one-pot protocol, in which eight tectoRNAs were mixed in equimolar concentrations, or a step-wise protocol, in which two nanosquares forming a polyhedron were assembled separately first. The transition from an RNA motif to 2D structures and then to 3D structures probably gave rise to a general method to build complex nanostructures. The same idea was also applied to obtain an RNA homo-octameric nanoprism (Figure 1.3B) which was made from an RNA square consisting of four RNA tiles (29). Furthermore, as tRNA is a natural component in cells, Jaeger's study demonstrated that small natural RNA as a building block can be applied to make complex architectures. Considering the large number of known small natural RNA motifs, RNA as a building block gives rise to the possibility to design and build many different shapes.

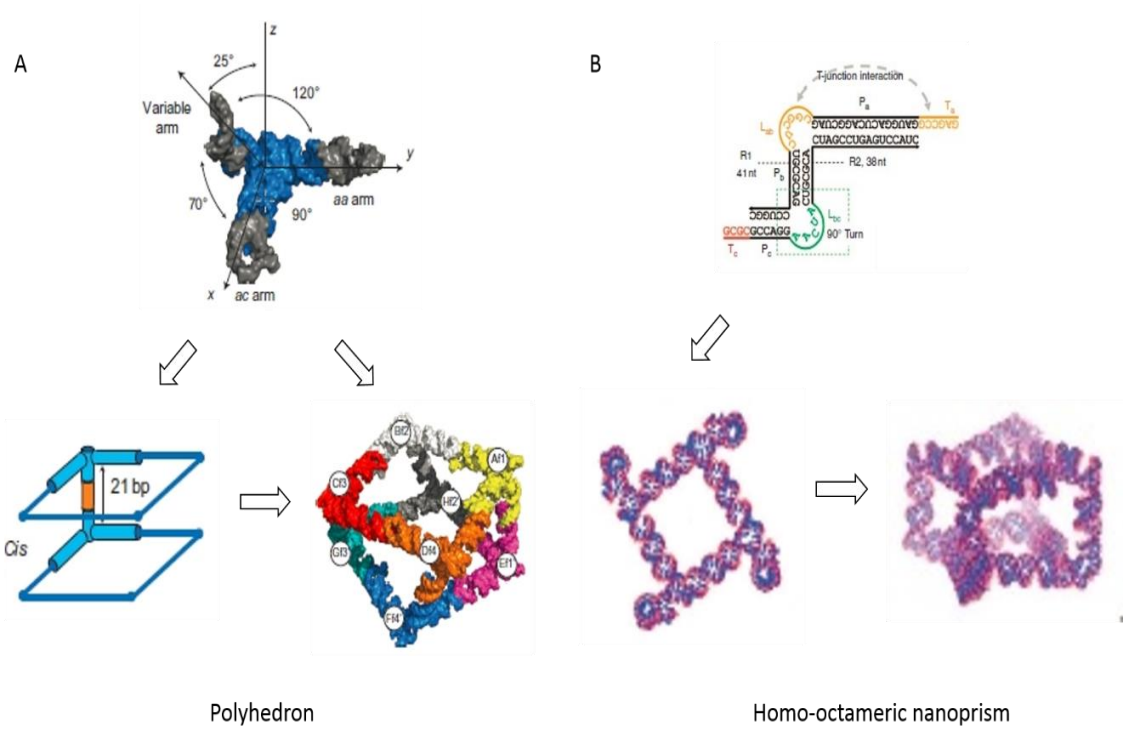

Figure 1.3 Three-dimensional RNA nanostructures. (A) A polyhedron made of tRNA from the ref. (28). The polyhedron can be prepared by either an one-pot protocol or a step-wise protocol in which two nanosquares forming a polyhedron were prepared first. (B) A homo-octameric nanoprism made from a designed, two-stranded RNA tile (R1–R2) from the ref. (29).

Pioneering work has also been done on RNA origami, a technique that folds single-stranded RNA into complicated pre-designed shapes. A similar concept has been successfully applied in DNA nanotechnology (30–32). In 2014, Cody Geary firstly reported several different RNA tiles with the largest nanostructure produced as a single strand comprised of 660 nucleotides and 35 helical subdomains (Figure 1.4) (33). These tiles were mediated by kissing loop, loop-loop complex and tetraloops from different RNA tertiary motifs instead of short staple strands in DNA origami. Researchers also tried other methods to build RNA tiles (34), but a general method for designing and building them has not been found yet.

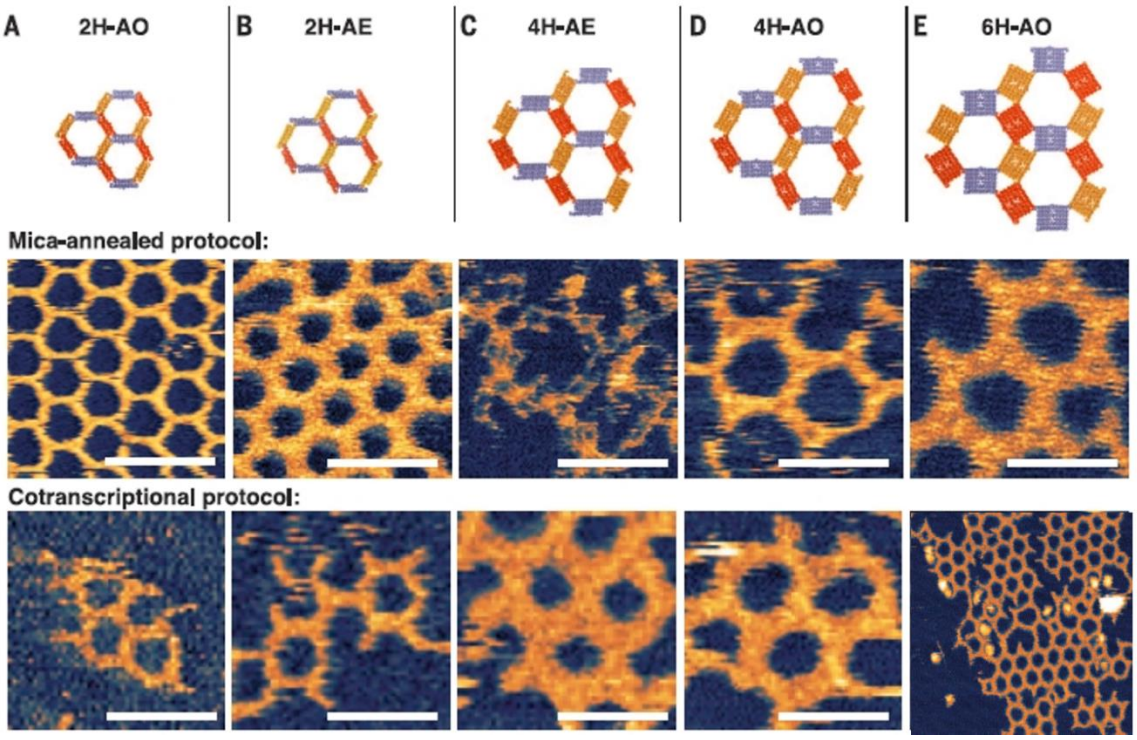

Figure 1.4 Different RNA tiles were made by involving kissing loops, loop-loop complex and tetraloops from different RNA tertiary motifs from the ref. (33). The largest RNA tile, 6H-AO, contained 660 nucleotides and 35 helical subdomains.

With great effort dedicated to RNA nanotechnology, diverse two-dimensional and three-dimensional RNA nanostructures have been successfully built, while building delicate, stable and functional RNA nanostructures from a small RNA motif remains a great challenge though. Without doubt, RNA nanotechnology is still in the early fancy stage and will be a constant research hotspot in the next decade.

1.3 Characterization

1.3.1 Polyacrylamide Gel Electrophoresis (PAGE) Assay

Gel Electrophoresis, extensively used in biology and biochemistry, is a method to separate proteins, DNA and RNA based on the charge, size and shape of molecules. The successful application of this technique to nucleic acids can be traced back to the 1960s when U. E. Loening reported successful separation of ribonucleic acid with high molecular weight by polyacrylamide gel in 1967 (35).

Polyacrylamide and agarose are two typical materials of gels. Unlike agarose gels that are able to separate a large range of nucleic acids, polyacrylamide gels, on the other hand, are typically applied for separation of proteins and small fragments of nucleic acids (5 to 500bp) since polyacrylamide gels have better resolving power than agarose gels (36, 37).

As shown in Figure 1.5, polyacrylamide is polymerized from acrylamide monomer and the cross-linking monomer N, N’-methylene bisacrylamide by radical polymerization with chemical initiators such as ammonium persulfate (APS) and tetramethylethylenediamine (TEMED). This reaction creates a mechanically stable gel because added bisacrylamide forms cross-links between two acrylamide polymer chains.

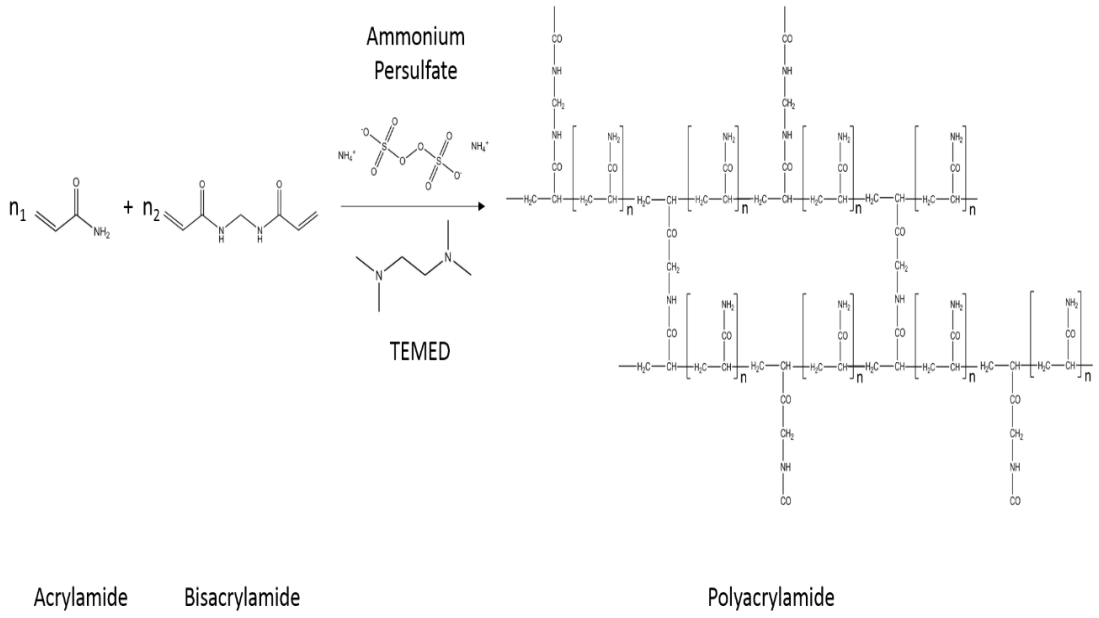

Figure 1.5 Polymerization of polyacrylamide from acrylamide and bisacrylamide initiated by ammonium persulfate (APS) and tetramethylethylenediamine (TEMED).

The percentage of polyacrylamide determines the resolving power of the resulting gel. Two parameters are important: total concentration of monomers (T%, in g/100ml) and weight percentage of cross-linkers (C%) (38).

$$T\% = \frac{g_{acrylamide} + g_{bisacrylamide}}{total\ volume, ml} \times 100$$

$$C\% = \frac{g_{bisacrylamide}}{g_{acrylamide} + g_{bisacrylamide}} \times 100$$

Increasing T% and C% both lead to a decrease in the average size of pores in the gel. The typical range of monomer concentration varies from 7.5% to 20% with different acrylamide/bisacrylamide ratios, such as 19:1, 29:1 and 37.5:1, corresponding to the cross-linker ratio of 5%, 3.3% and 2.6%, respectively. The best separation for analysts can be achieved by varying these

two parameters. A general guide for choosing the concentration of monomers is given in Table 2.

Table 2. Molecular weight separation guide-lines for uniform concentration gels (39)

Acrylamide Concentration		Molecular Weight of Sample
T%	C%	
5	2.6	25000—300000
10	2.6	15000--1000000
10	3	1000--100000
15	2.6	12000--50000
3.3-20	2	14500--2800000
3--30	8.4	13000--1000000
5--20	2.6	14000--210000
8--15	1	14000--330000

1.3.1.1 General Principles of Gel Electrophoresis

The term ‘gel’ refers to a highly cross-linked polymer which serves as a material to separate the target molecules. This separation is achieved by numerous pores inside the gel since relatively smaller molecules move faster through the pores than large molecules. The term ‘electrophoresis’ refers to the electromotive force (EMF) which is an external force provided by an electronic potential that moves charged molecules through the gel. Therefore, gel

electrophoresis is a process which enables the separation of charged molecules by applying electromotive force.

1.3.1.2 Apparatus

As shown in Figure 1.6, the apparatus for polyacrylamide slab gels includes two parts: a power source which provides electronic force and a gel box which contains gels and buffer.

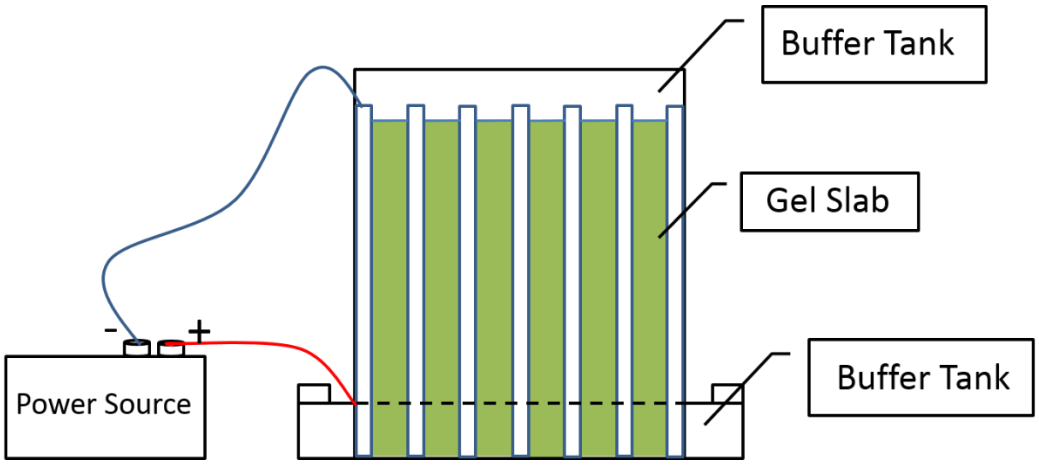

Figure 1.6 Scheme of apparatus for native gel

The gels are usually cast between two glass plates which are held apart by plastic strips, and a comb is inserted at the top of gel to create several wells. Subsequently, the thickness of the plastic strips and the comb determines the thickness of the gels which has an impact on the amount of sample that can be loaded. Before the gel electrophoresis process starts, the gel between two glass plates is inserted into the buffer tank, soaking in an environment of specific buffer which enables the sample remaining stable during the electrophoresis process.

Then, different samples are loaded into adjacent wells and run parallel in the separate wells.

1.3.1.3 Denaturing Gel and Native Gel

With the requirement to obtain unambiguous data, the natural structure of DNA and RNA affecting the mobility of macromolecules in the gel needs to be disrupted, forcing them to unfold into linear chains. Under this circumstance, a denaturing gel is a necessity.

The disruption of a structure is realized by a denaturing agent in the gel. Urea, a diamide of carbonic acid (Figure 1.7), is the most widely applied denaturing agent for nucleic acids. It competes with H-bonds between DNA and RNA bases by hydrogen bonding with them, preventing the formation of Watson-Crick pairs between bases (40).

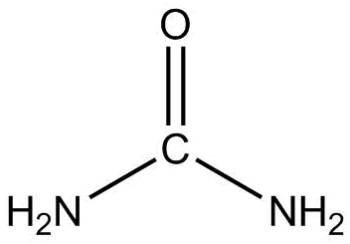

Figure 1.7 Structure of urea.

In contrast, in native gels which contain no denaturing agents, nucleic acids retain their natural structure. Hence, in native gels, biomolecules are separated based on molecular weight, charge, as well as shape. This technique

is widely applied in detecting self-assembling RNA nanostructures which are prepared relying on the intrinsic structure of RNA.

1.3.2 Förster Resonance Energy Transfer (FRET) and Fluorescence Quenching Assay

1.3.2.1 Förster Resonance Energy Transfer (FRET) Assay

FRET is a technique which has been widely used to observe inter- and intra-molecular interactions. It describes a mechanism that light energy is transferred from a donor chromophore to a nearby acceptor chromophore through non-radiative dipole-dipole coupling (41). The efficiency of this energy transfer, referring to the ratio of acceptor intensity to total emission intensity, is described by the following equation (42):

$$E = (1 + (R / R_0)^6)^{-1}$$

where E is the efficiency of energy transfer, R is the distance between two chromophores, and R_0 is the Förster radius at which $E = 0.5$ (Figure 1.8).

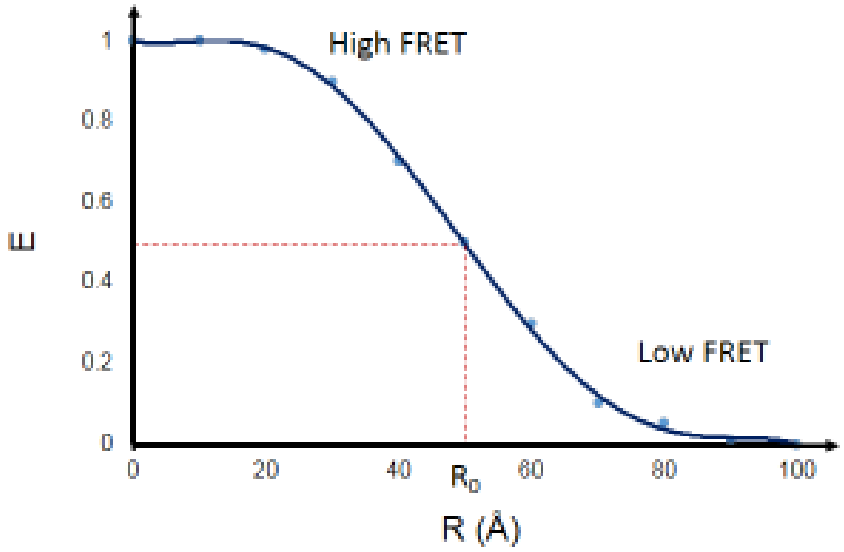

Figure 1.8 FRET efficiency (E) as a function of distance (*R*) between two dyes. In this figure, R_0 is set at 50Å. At $R=R_0$, E=0.5.

Since the efficiency of energy transfer is inversely proportional to the sixth power of the distance between two chromophores, FRET efficiency is extraordinary sensitive to tiny changes in the distance between donors and acceptors, and because of that, FRET is able to detect intra-molecular reactions, such as conformational changes in one molecular (43), as well as inter-molecular reactions (44).

Cy3 (Figure 1.9A) and Cy5 (Figure 1.9B), both belonging to cyanine dye family, are a widely used fluorophore pair for FRET experiments since cyanine dyes became commercially available in 1990s (45–47), because these dyes have well-separated emission spectra as well as appreciable overlap between donor (Cy3) emission and acceptor (Cy5) absorption (48). Cy3 is excited at 550nm and emits at 570nm, while Cy5 is excited and emits at 650nm and 670nm respectively. The Förster Radius (R_0) for the Cy3-Cy5 pair is 6nm (49).

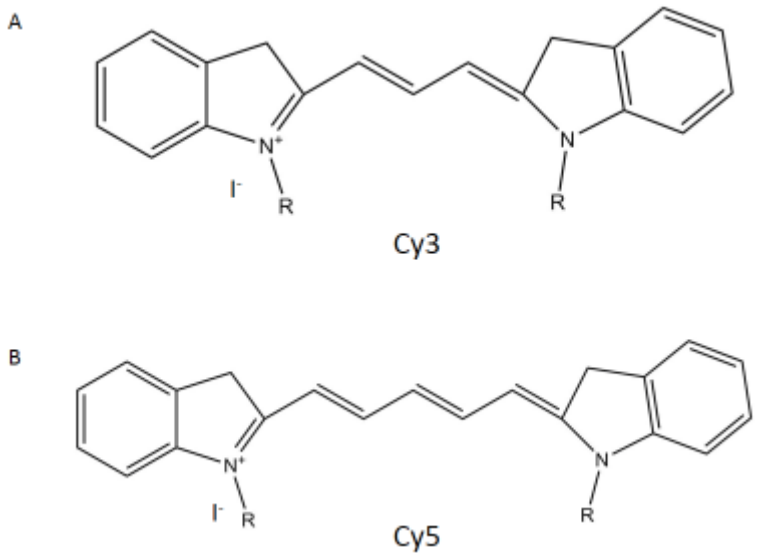

Figure 1.9 Structure of Cy3 (A) and Cy5 (B)

1.3.2.2 Fluorescence Quenching Assay

Quenching is a process that reduces the fluorescence intensity from a fluorophore, which is achieved by the dark quencher, a substance that efficiently absorbs energy from an excited fluorophore in a broad wavelength range. Therefore, in the fluorescence quenching experiment, a fluorophore acceptor in the FRET is replaced by a dark quencher, constituting a fluorophore-quencher pair. In the Cy3-Cy5 pair, Cy5 emits light by absorbing energy from excited Cy3 when the dye pair is within a certain distance. In a fluorophore-quencher pair, however, the fluorophore's emission is suppressed when they come close. More specifically, the excited dye returns to the ground state by transferring energy to a nearby quencher without emitting light. The excited quencher then returns to the ground state by emissive decay or dark quenching instead of emitting light (50). This effect has also been widely applied in monitoring conformational changes and reactions at molecular level (51, 52).

1.3.3 Atomic Force Microscopy (AFM) Assay

Atomic force microscopy (AFM) is a kind of scanning probe microscopy with ultra-high resolution, which is over 1000 times better than that of an optical microscopy, giving rise to a resolution on the order of nanometers. This technique was invented in the early 1980s and applied in scientific research immediately (53).

The configuration of an AFM instrument is shown in Figure 1.10. The core component of the AFM instrument is a cantilever with a probe tip which scans the specimen surface. The cantilever is deflected by the interaction between the sample's surface and the probe tip when the tip is brought close to the surface. This deflection following Hooke's Law and produces an AFM image when mapped over a surface area (54). Other important components include a stage for samples, an xyz drive to displace the sample, a piezoelectric element to oscillate the cantilever, and a laser emitter and photodiode for signal registration.

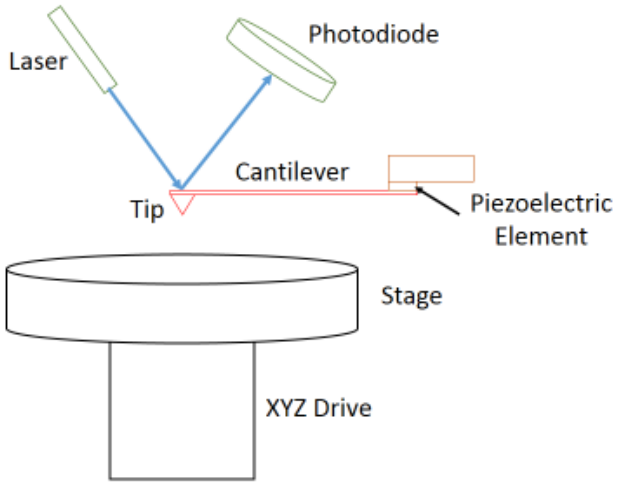

Figure 1.10 Configuration of an AFM instrument

Apart from measuring force and manipulating the properties of samples in a controlled way, imaging as the basic function for every microscopy technique is of great importance in the field of RNA nanotechnology. RNA nanostructures form particles between 1 to 10 nanometers which are difficult to be characterized by scanning electro-microscopy (SEM).Transmission electronic microscopy (TEM) is capable to image at the order of nanometers, but it is only capable to provide a two-dimensional image rather than a three-dimensional image. AFM is able to form a three-dimensional image at a high resolution by recording the height of the probe. When AFM is taking an image of a sample, the probe carried by the cantilever scans over the surface of the sample and the detector records the height of the probe corresponding to a constant force interaction between probe and sample. This constant interaction that the sample imposes on the probe is used to calculate a three-dimensional image (topography) at a high resolution.

A key step to imaging RNA nanostructure is to stabilize the sample on a substrate. Among several materials that have been developed as a substrate, mica is the most widely applied one owing to its ultra-smooth surface (55–57). Surface modification by forming a positive charged substrate is required to stabilize negatively charged nucleic acids. Common methods are cation-assisted modification by incubating the substrate in a solution containing cations such as Mg^{2+}, and chemical modification which controllably modifies the surface by a chemical reaction (58).

The operation of the tip in the AFM instrument may be achieved in three distinct modes: contact mode, non-contact mode and tapping mode. The last one is most widely applied in imaging nucleic acids (59–62) and other ambient or liquid surface (63, 64). In the tapping mode, the probe tip goes down close enough to the sample's surface while still keeping a certain distance from the surface. The cantilever, which is driven by the piezoelectric element, oscillates at a certain frequency and amplitude which remains constant as long as no interaction with the sample's surface is encountered. After the cantilever dragging the tip comes close to the surface, intermolecular forces, such as van der Waals forces, cause a change in the amplitude of oscillation which is recorded by the AFM instrument. An AFM image in the tapping mode is therefore produced by recording the change in amplitude as the tip scans over the surface (65).

AFM has been widely applied to observe DNA and RNA nanostructures, such as DNA junctions (66), RNA arrays (67), etc. In the foreseeable future, with the development of RNA nanotechnology, AFM will keep playing a dominant role in characterizing small structures that are made of ribonucleic acids.

Chapter 2. Goal of Project

RNA switches are found in mRNA and control gene expression by binding ligands to change expression of the mRNA (68, 69). RNA switches adopt specific structures, such as the subdomain IIa switches in the internal ribose entry site (IRES) of hepatitis C virus (HCV) and Seneca Valley virus (SVV), which were previously analyzed by X-ray crystallography (70–72). Structural analysis determined a unique 90° bend in the IIa domain of both HCV and SVV. Based on the crystal structure of these viral RNA switches, a self-assembling RNA square and triangle have been successfully designed and prepared (Figure 2.1).

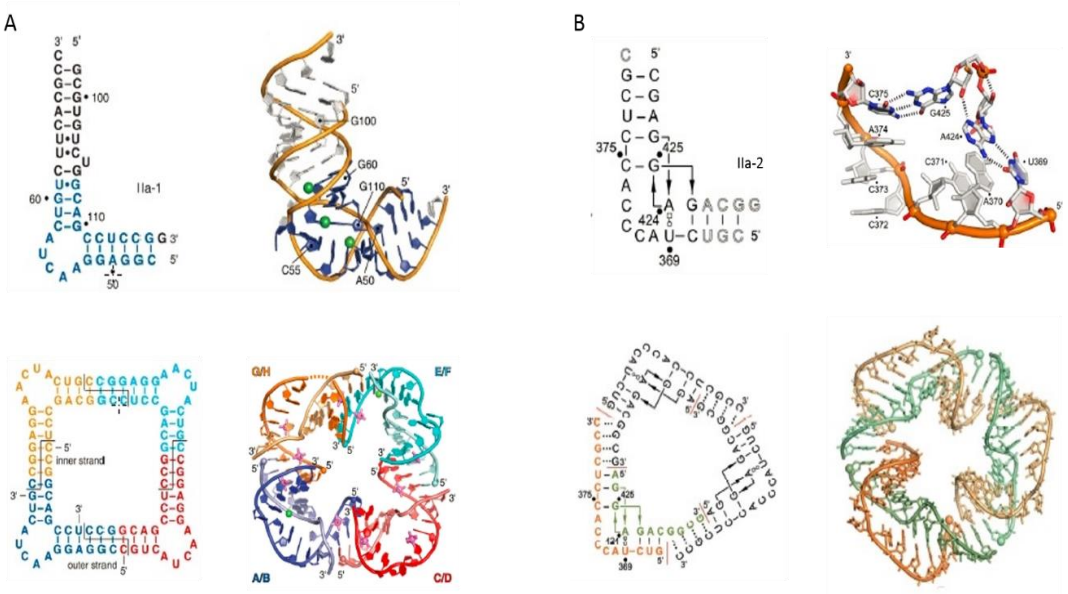

Figure 2.1 Design of self-assembling RNA nanosquare and nanotriangle. (A) The sequence and structure of IIa-1 RNA represent the IIa subdomain in the IRES from HCV which was used to prepare the RNA nanosquare from IIa-1 RNA. (B) The sequence and structure of the IIa-2 representing IIa subdomain in the IRES from SVV which was used to prepare the RNA nanotriangle from IIa-2 RNA.

We assumed that a triangular nanoprism, a structure that has not been made yet in the field of RNA nanotechnology, can be rationally designed and made in two steps: the first step was to extend the original nanotriangle with a certain length of single-stranded overhangs; the second step was then to combine two extended triangles by DNA or RNA splints which connected to the triangles by hybridization with the overhangs (Figure 2.2A). The overhangs were connected to the original triangle by a single uracil or a non-nucleoside spacer (Figure 2.2C) which did not participate in interaction with the splints and enable overhangs to move and rotate flexibly. The extension of the nanotriangle and the formation of nanoprism were investigated by native PAGE, and the nanoprism was further studied by FRET, fluorescence quenching methods and AFM.

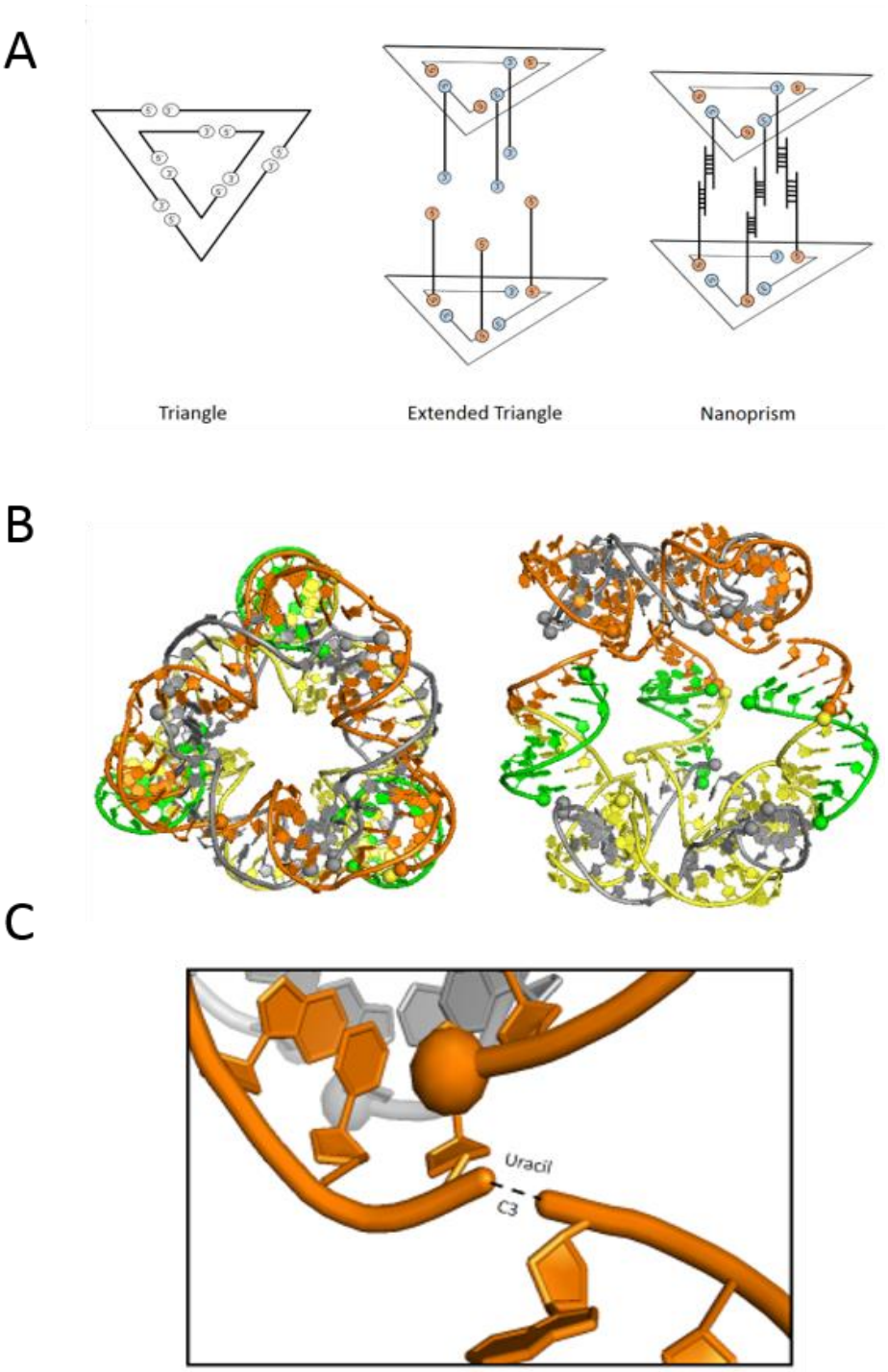

Figure 2.2 Scheme and model of the nanoprism. (A) Scheme of the RNA nanoprism made from nanotriangles in two steps: 1) RNA nanotriangle was extended with overhangs. 2) Two extended triangles were connected by DNA or RNA splints. (B) Three dimensional model of the nanoprism: top view is on the left; front view is on the right. (C) Detail view showing the uracil and C3 spacer linker between RNA overhangs and the triangle.

Chapter 3. Native PAGE Analyses

As described previously, native PAGE is able to separate RNA based on the size of molecules since a relatively large construct typically migrates slower than the small one in the gel electrophoresis. Therefore, PAGE analysis is able to give a general thought about the formation of an RNA nanoprism since the nanoprism is larger than the original triangle.

3.1 Extension of the Original Triangle

3.1.1 Modification from Inner Strands

The first attempt to modify the original triangle was to extend the inner strands by 5 nucleotides connected via a single uracil as the linker (Figure 3.1). The linker was designed to make overhangs flexible and reduce the interference caused by the strand extensions.

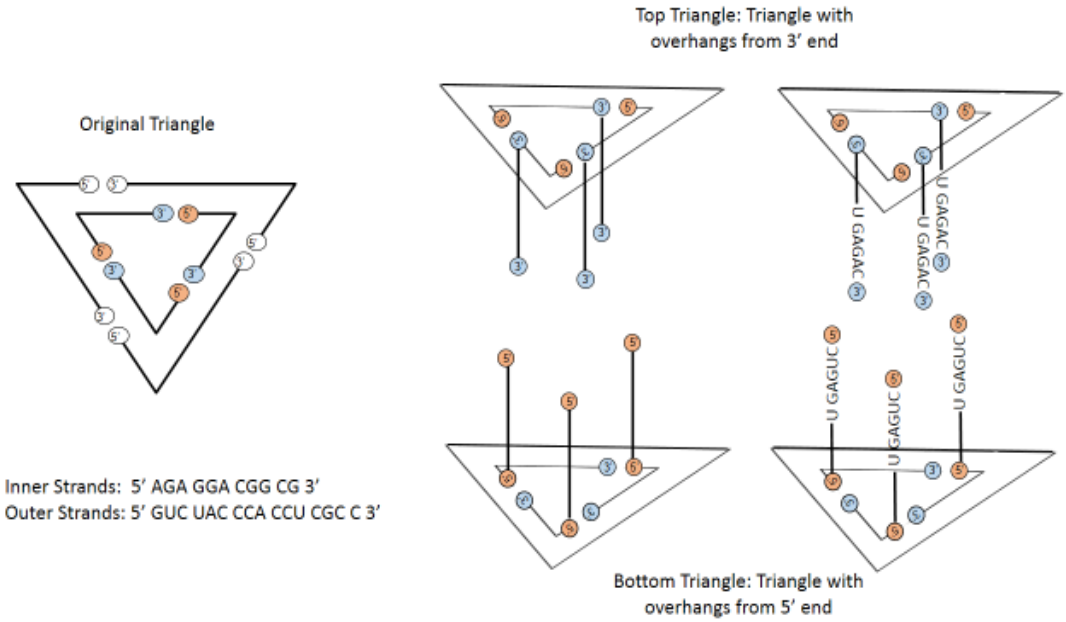

Figure 3.1 Scheme of the extended triangles with modification from the inner strands of the original triangle. The sequence of overhangs from the 3' end and 5' end is GAGAC and GAGUC, respectively. A single uracil was incorporated as a linker.

Inner and outer strands were annealed in 10mM Mg^{2+} buffer by heating up to 65ºC and then incubating at 37ºC for 10 minutes before cooling down to 5ºC. PAGE analysis (Figure 3.2) indicated that both top and bottom triangle did not form. More specifically, two single extended inner strands (3' Inner and 5' Inner) migrated similarly, consistent with their sizes (both 21-nt). The double strands (3' Inner + Outer and 5' Inner + Outer), however, moved much faster than the original triangle, demonstrating that the extended inner strands base paired with the outer strands to form a corner of a triangle instead of a complete triangle. A possible reason for the failure might be that the gap between 3' and 5' end of the inner strands in the triangle structure was too narrow to accept extensions. In other words, the extending nucleotides prevented the isolated corners from

moving towards to each other to form a complete triangle. Another possible reason for the failure might be competing structure formation of the inner strands with extensions from the 5’ end which showed a smeared band in the gel. By analyzing the sequence, the 5’ extended inner strands were found to show a propensity for the formation of a dimer or a hairpin structure which may also interfere with the formation of the extended nanotriangle.

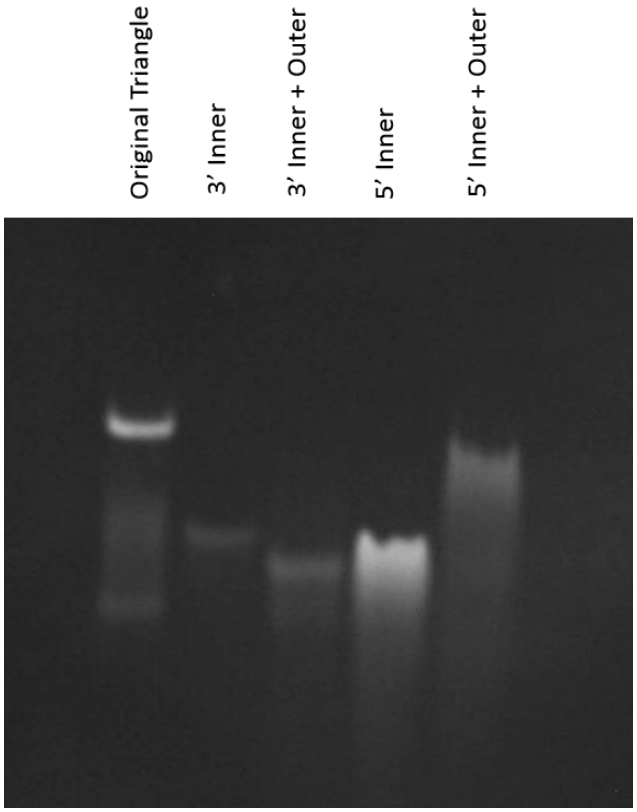

Figure 3.2 PAGE analysis of the structure modified by extending the inner strands of the original triangle. The native gel was set in the presence of 10mM Mg^{2+}.

3.1.2 Modification from Outer Strands

The second attempt was to extend the outer strands of the original triangle. The basic concept (Figure 3.3) remained the same, while the length and sequence of the overhangs, as well as the linkers, varied.

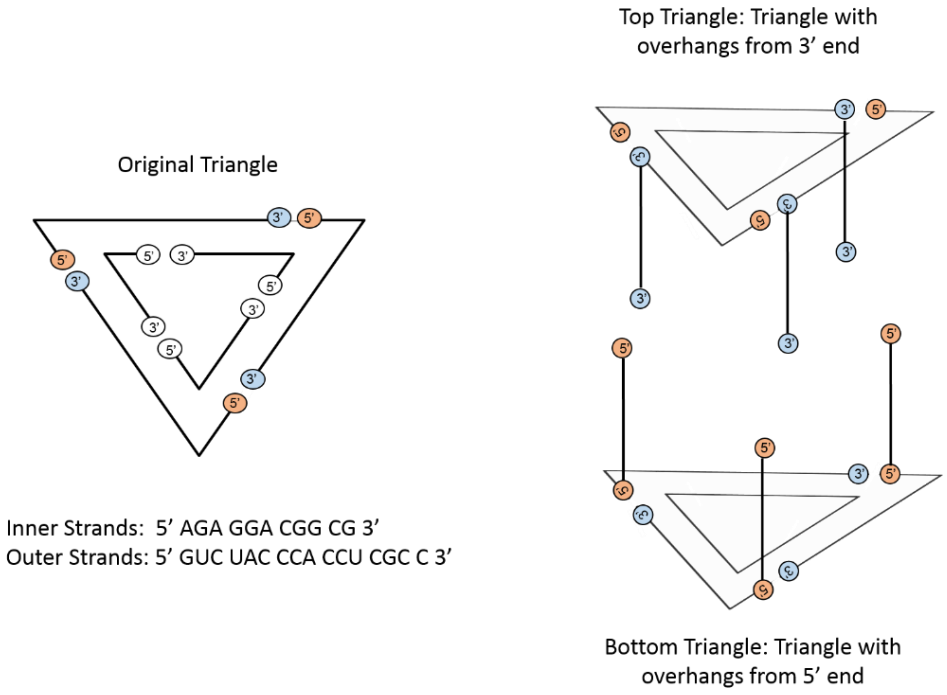

Figure 3.3 Scheme of the extended triangles with overhangs extending from the outer strands of the original triangle.

3.1.2.1 Modification of the Outer Strands with a uracil as a Linker

Extension with a single nucleotide at the 3’ end of the outer strands (3’ Outer-one) was tested by PAGE first. The extended construct carrying three nucleotides were found to migrate slower than the original triangle in the gel, suggesting that a larger triangle was formed. The band appeared to be smeared,

which was supposedly caused by the three dangling nucleotides. This result indicated that the gap between the ends of two outer strands was larger than that of the inner strands, which was also revealed by the crystal structure of the original triangle (25). Successful modification with one nucleotide led to the next step which was to extend the triangle with longer overhangs from the outer strands.

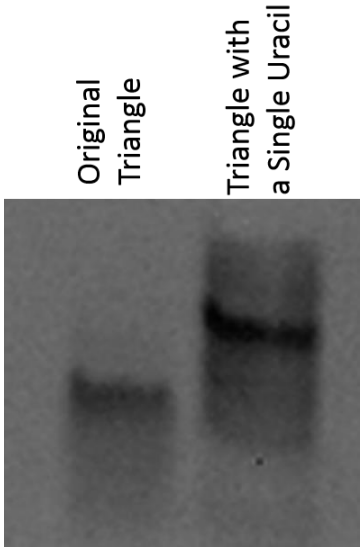

Figure 3.4. PAGE analysis of the new construct which contained a single nucleotide as overhang.

Subsequently, two new outer strands with five nucleotides as overhangs, one extended from the 3’ end and the other extended from the 5’ end, were designed (see the sequence in Materials and Methods part in Chapter 3). However, it turned out that these two new outer strands were not able to form extended triangles. PAGE analysis (Figure 3.5) clearly showed that all single strands (5’ Outer-1 and 3’ Outer-1) and double strands (5’ Outer-1 + Inner and 3’ Outer-1 + Inner) migrated much faster than the original triangle, indicating that

the double strands formed an isolated corner instead of a complete triangle again. Several separate bands shown in the last well corroborated this conclusion. In this well, the inner strands and the two extended outer strands were mixed with the DNA splint-1. The top band which migrated similarly to the original triangle was a construct that was a combination of two corners with a DNA splint. This construct included 76 nucleotides which were about the same number as that in the original triangle (81-nt). The separate bands beneath the top band represented single corners which were not connected by DNA splints.

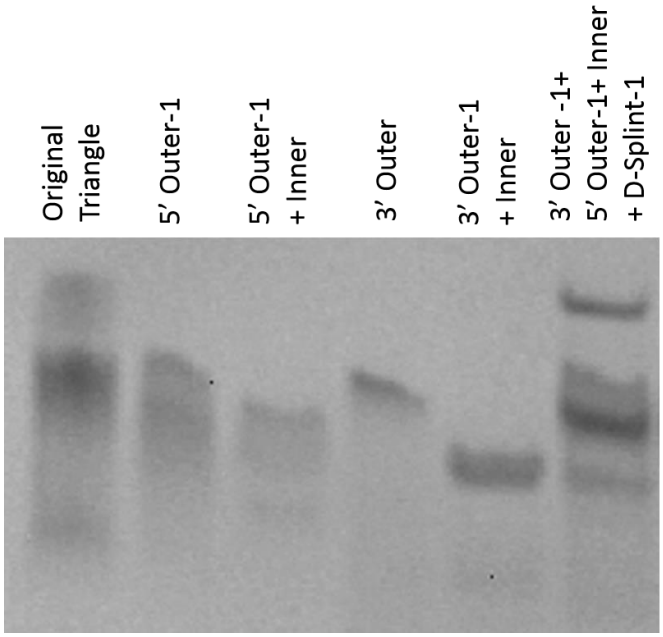

Figure 3.5 PAGE analysis for the attempt to extend outer strands with 5 nucleotides as overhang

3.1.2.2 Modification of the Outer Strands with a C3 Spacer as Linker

The C3 spacer is a non-nucleoside three-carbon spacer (Figure 3.6) that is used to incorporate a flexible linker into an oligonucleotide. It has long been

applied in DNA and RNA functional studies by incorporating at the end or in the middle of an oligonucleotide(73, 74). Here, the goal of introducing a C3 spacer was to provide more flexibility to the overhangs than that provided by a uracil linker.

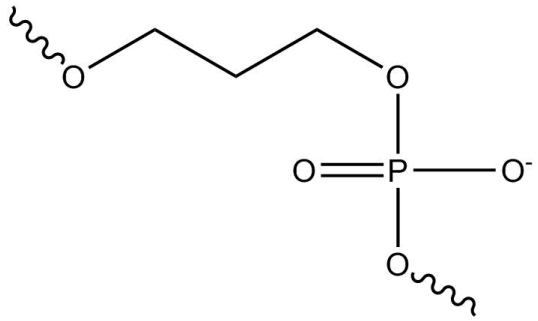

Figure 3.6 Structure of C3 spacer

With incorporating a C3 spacer, two new outer strands with the overhang containing five nucleotides (see the sequence in the Materials and Methods part in Chapter 3) from 3’ and 5’ end (3’ Outer-2 and 5’ Outer-2), respectively, were designed. The result (Figure 3.7) showed that two new triangles with three overhangs both appeared as a dominant band which migrated slower than the original triangle, clearly indicating the formation of extended triangles. Moreover, migration of the two new triangles were found to be similar, which were consistent with their sizes (both 96-nt).

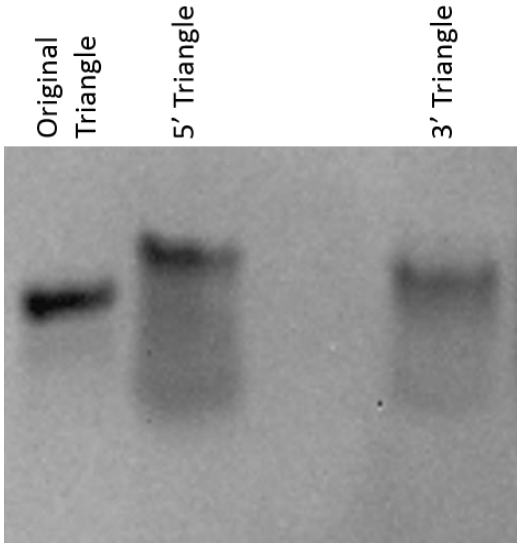

Figure 3.7 PAGE analysis of two new extended triangles with 5 nucleotides as overhang from outer strands of the original triangles. The gel contained 20mM Mg^{2+}.

The successful formation of two new extended RNA nanotriangles owed to the incorporation of the C3 spacer. Compared with a single nucleotide, the C3 spacer as a linker provided more flexibility to the overhangs, facilitating to direct them out of the plane of the triangle. Therefore, three individual corners composed of one inner strand and one outer strand were capable to form a complete triangle without the interference of overhangs. The new sequence of overhangs might also contribute to the formation of the triangle by removing the competing dimer or hairpin structure from the extended outer strands.

Table 3. PAGE analysis results for every attempt to extend the original triangle ('×' means failure, '√' means success, 'n.d.' means not determined)

Extended from inner strands		Extended from outer strands			
uracil as linker		uraicl as linker		C3 as linker	
one nucleotide extension	five nucleotides extension	one nucleotide extension	five nucleotides extension	one nucleotide extension	five nucleotides extension
×	×	√	×	n.d.	√

To sum up, all previous PAGE analyses (shown in the Table 3) explored the possibility to modify a designed nanotriangle made entirely of double-stranded RNA with short oligonucleotides as overhangs. The results clearly indicated that modifications from inner strands of RNA nanotriangle were not tolerated likely due to the narrow gap between the 3' and 5' end. Further investigation proved that the narrow gap between the 3' and 5' end cannot tolerate even a single nucleotide extension, which, in return, demonstrated that the originally designed nanotriangle is extremely compact.

Modifications from outer strands appeared to be feasible because of larger gap between the two strand ends, which was also consistent with the crystal structure of the nanotriangle (25). Successful modification with overhangs containing five nucleotides, however, still required to incorporate a non-nucleoside three-carbon spacer to provide extra-flexibility to the overhangs. The C3 spacer directed the overhangs, which were able to move and rotate flexibly,

out of the plane of the triangle so that the new triangle was able to form without the interference of the overhangs.

3.2 From the Extended Triangle to the Nanoprism

After the formation of the extended triangles, the next step was to form the nanoprism by combining the overhangs from extended triangles with DNA splint-2 (10-nt). The most straightforward method was to mix every component at once. In this one-pot protocol, stocking solution of 2μL inner strands, 1μL outer strands with overhangs from the 5' end, 1μL outer strands with overhangs from the 3' end and 2μL DNA splints-2 at equal molar ratio were mixed with a reaction buffer containing 20mM Mg^{2+}. The mixture was heated up to 65ºC for 5 minutes, and then incubated at 37ºC for 10 minutes followed by cooling down to 5ºC. From the PAGE analysis (Figure 3.8), the shift from the original triangle to a band that may represent the final nanoprism can be seen clearly. More specifically, the overhangs from the end of the triangle stably base paired with DNA splints to form a larger structure (5' triangle + splint and 3' triangle + splint, both 121-nt) than the single triangle (5' triangle and 3' triangle, both 96-nt), indicating that DNA splints had a potential to combine two triangles to form the desired nanoprism. The nanoprism (222-nt) showed a main band which migrated slower than all previous bands, which suggested the formation of the nanoprism. However, this main band appeared to smear in the gel, indicating that the new three dimensional construct was not of high stability. Another possible reason for

that smeared band was the presence of by-products, such as a single extended triangle with DNA splints, which were also formed during the one-pot process.

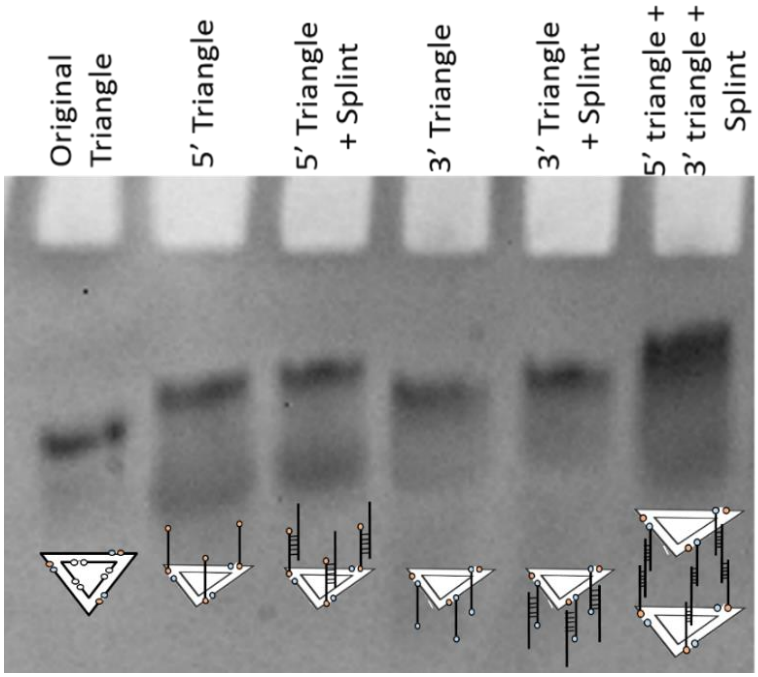

Figure 3.8 PAGE analysis of nanoprism containing DNA splints with cartoon images of proposed RNA species. The gel was run in the presence of 20mM Mg^{2+}.

In order to build a more stable construct, the DNA splints were replaced by RNA splints, while the length of the splints remained the same (10-nt). Furthermore, a step-wise protocol was designed to assemble the nanoprism, in which two extended triangles were prepared separately first, and then the two extended triangles were mixed with the RNA splints at 37ºC. This strategy not only provided further evidence for the formation of the nanoprism, but also avoided some unexpected structures as by-products which potentially formed in the one-pot protocol, such as a triangle containing overhangs both from 3' and 5' ends.

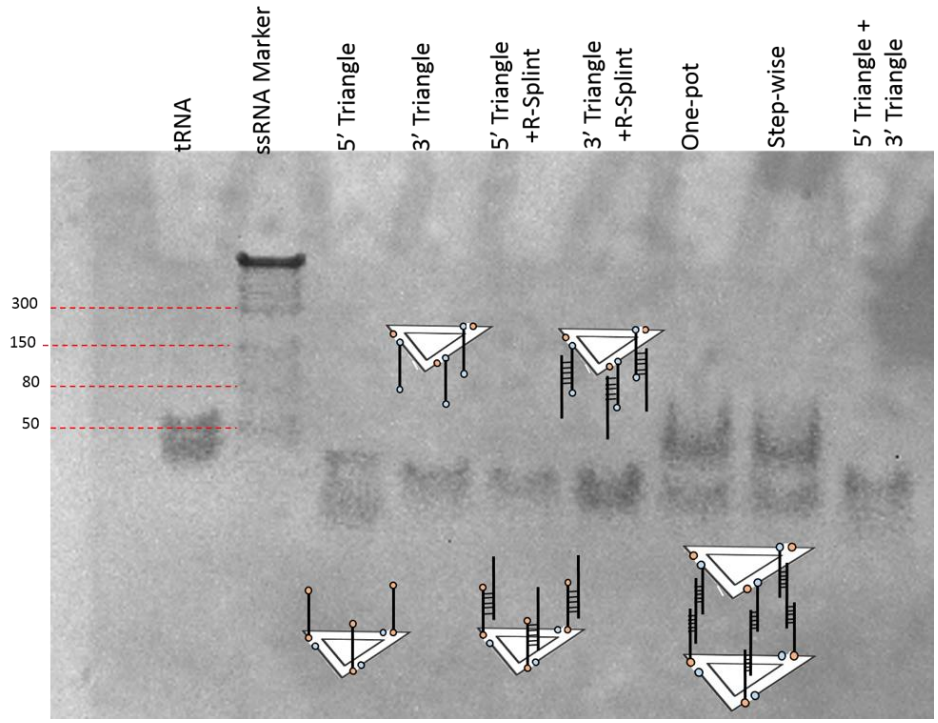

Figure 3.9 PAGE analysis of RNA nanoprism incorporated with RNA splints and showing cartoon images of proposed RNA species. The gel was run in the presence of 20mM Mg^{2+}.

The PAGE analysis result is shown in Figure 3.9. Unlike previous results obtained from mixtures containing DNA splints, the shift from a single extended triangle to a single extended triangle base paired with RNA splints disappeared, indicating that the construct containing RNA splints were extremely compact. This compactness might be an attribute for the formation of a stable prism. As shown in Figure 3.9, the nanoprism, either prepared by the one-pot or the step-wise protocol, exhibited the same defined band in the gel, demonstrating that two different protocols resulted in the same structure. These two defined bands not only migrated slower than the constructs containing a single triangle with splints (5' Triangle + R-splint and 3' Triangle + R-splint), but also significantly slower

than the band representing the physical combination of two different triangles without splints (5’ Triangle + 3’ Triangle). The latter faster moving band was a persuasive evidence to suggest that two extended triangles were combined by the RNA splints to form a nanoprism. It is also worth noting that the second weak band observed in the one-pot and step-wise samples may represent constructs, such as the extended triangles, that were not involved in the formation of the nanoprism. These unreacted constructs can be seen again in the AFM images shown in Chapter 5. Interestingly, all these constructs, including the single extended triangle (96-nt) and the nanoprism (222-nt), all migrated slower than the 50-mer ssRNA marker, demonstrating that all these constructs were extremely compact. This result was also in a good agreement with the result that showed the formation of the original triangle in a previous report (25).

Gel evidence suggested that the nanoprism was built by combining two extended triangles with DNA or RNA splints, but the construct with RNA splints were more compact and stable. The compactness might be due to the difference in hybrid structures between DNA and RNA chains. The 2’ hydroxyl group in the RNA ribose induces a 3-endo chair conformation in the sugar ring, resulting in the RNA double helix A-form, which is shorter than the B-forms that the DNA double helix favors, as well as the form that presents in the DNA-RNA double helix (75). The A-form conformation of the RNA double helix resulted in the compactness of the nanoprism containing RNA splints. The stability might be owing to formation of thermodynamically stable RNA-RNA base pairs. Gibbs free energy measurements revealed that base paring in RNA-RNA double strands

provides the thermodynamically most stable interaction compared to DNA-DNA pairs and DNA-RNA hybrid pairs.

Gel evidence also showed that the nanoprism was able to be prepared in either an one-pot protocol or a step-wise protocol. The multiple paths to form the nanoprism from the single oligonucleotides mutually corroborated the formation of the RNA nanoprism, but also exhibited the successive transition from single oligonucleotides to 2D constructs and then to 3D constructs. The same idea was previously used to build a polyhedron (28) and homo-octameric nanoprism (29), indicating this path of successive assembly is indeed a general method to build complex three dimensional constructs from RNA oligonucleotides.

3.3 Materials and Methods

Materials:

Oligonucleotides: All RNA and DNA strands were purchased from IDT, Inc.

Inner strands of the original triangle: 5’ AGA GGA CGG CG 3’. Outer strands of the original triangle: 5’ GUC UAC CCA CCU CGC C 3’.

Modification from the inner strand: 3’ Inner: 5’ AGA GGA CGG CGU GAG AC 3’. 5’ Inner: 5’ CUG AGU AGA GGA CGG CG 3’.

Modification from the outer strand with a uracil as the linker: 3’ Outer-one: 5’ GUC UAC CCA CCU CGC CU 3’. 3’ Outer-1: 5’ GUC UAC CCA CCU CGC CUG AGA C 3’. 5’ Outer-1: 5’ CUG AGU GUC UAC CCA CCU CGC C 3’.

Modification from the outer strand with C3 spacer as the linker: 3’ Outer-2: 5’ GUC UAC CCA CCU CGC C/C3/CU GUC 3’. 5’ Outer-2: 5’ CAC AC/C3/G UCU ACC CAC CUC GCC 3’.

DNA splint-1: 5’ CUC AGG UCU C 3’. DNA splint-2: 5’ GTG TGG ACA G 3’. RNA splint: 5’ GUG UGG ACA G 3’.

Methods:

Formation of the extended triangles with uracil as a linker: two RNA strands (one inner and one outer) at 200μM were mixed in the reaction buffer containing 125mM Na^+ and 10mM Mg^{2+}. The mixture was incubated at 65ºC for 5 minutes, 37ºC for 10 minutes and 5ºC for 5 minutes.

Formation of extended triangles with C3 spacer as a linker: two RNA strands (one inner and one outer) at 200μM were mixed with reaction buffer containing 125mM Na^+ and 20mM Mg^{2+}. The mixture was incubated at 65ºC for 5 minutes, 37ºC for 10 minutes and 5ºC for 5 minutes.

One-pot protocol to form nanoprism: 2μL inner strands, 1μL 3’ Outer-2 strands, 1μL 5’ Outer-2 strands, and 2μL DNA splint-2 at equal molar ratio (150mM) were mixed in reaction buffer containing 125mM Na^+ and 20mM Mg^{2+}. The mixture was heated up to 65ºC for 5 minutes and then incubated at 37ºC for 10 minutes before cooling down to 5ºC.

Step-wise protocol to form nanoprism: two extended triangles were first self-assembled according to a similar procedure to form extended triangles.

Before cooling down to 5ºC, two extended triangles were mixed with RNA splints in reaction buffer containing 125mM Na^{+} and 20mM Mg^{2+}. The mixture was incubated at 37ºC for another 10 minutes followed by cooling down to 5ºC.

Native PAGE: 8% polyacrylamide gel was prepared with 19:1 acrylamide/bisacrylamide buffer and 20mM Mg^{2+} buffer. The gel was operated at ice temperature, 22mA current and 220V voltage.

Chapter 4. Förster Resonance Energy Transfer (FRET) and Fluorescence Quenching

4.1 Förster Resonance Energy Transfer (FRET)

To further investigate the structure of the RNA nanoprism, a FRET assay was established in a 96-well format. Therefore, we designed two new DNA splints (the sequence remained the same as the DNA splints-2 in the Chapter 3, see details in the Materials and Methods part in the Chapter 5) modified with a pair of terminally conjugated cyanine dyes. One splint was labelled with a Cy3 dye and the other one with a Cy5 dye. According to the crystal structure of the original nanotriangle, the sites in the nanoprism chosen for dye conjugation were at a distance that enables FRET to occur at a high efficiency.

Figure 4.1A shows the FRET signal from the sample containing two extended triangles and the two DNA splints with a pair of cyanine dyes. This sample exhibited strong FRET signal which increased dramatically with an increasing Mg^{2+} concentration, suggesting that the formation of the nanoprism required high Mg^{2+} concentration. However, further investigation (Figure 4.2B, Cy3+Cy5) revealed that the mixture of only two DNA splints also exhibited high FRET signal. Further inspection of the splint sequences showed that one DNA splint was able to base pare with the other one to form a dime. This dimer was disrupted to some extent by the outer strands from two extended triangles,

resulting in a slight decrease of the FRET signal (Figure 4.2B, No Inner). Since we cannot distinguish if the FRET signal (Figure 4.1A) derives from the nanoprism or the splint dime, the result from the magnesium titration was inconclusive.

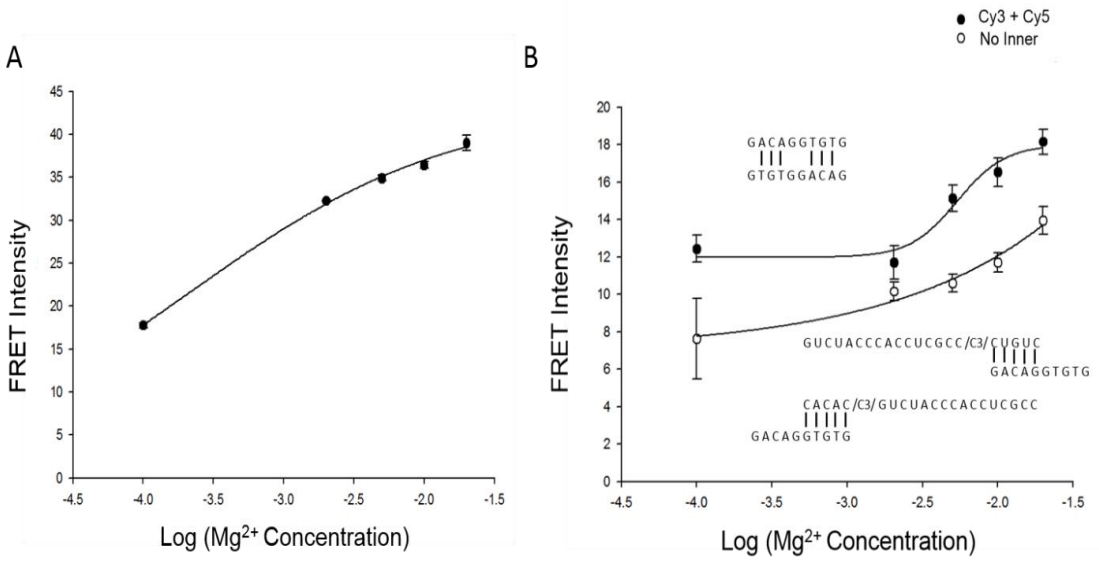

Figure 4.1 FRET experiment. (A) The sample containing two extended triangle and two DNA splints with a pair of cyanine dyes was titrated with Mg^{2+} from 0mM to 20mM. (B) The sample containing two DNA splints and the sample containing two DNA splints and two outer strands of the extended triangles were both titrated with Mg^{2+} from 0mM to 20Mm.

4.2 Fluorescence Quenching

In order to reduce the background signal from the unexpected dimer structure, an RNA splint (the sequence remained the same as the RNA splint in the Chapter 3, see details in the Materials and Methods part in the Chapter 5) with a Cy5 dye and a DNA complementary splint with a black hole quencher (BHQ-2) were introduced. BHQ-2 is a commercially available quencher that is able to suppress the emission of Cy3 and Cy5 dyes. The DNA complementary

splint was designed to form a hybrid with the RNA splint involving 6 consecutive base pairs. Therefore, when the RNA splint and the DNA complementary splint are mixed, heterodimer formation between the splints is expected to result in quenching of the cyanine fluorescence.

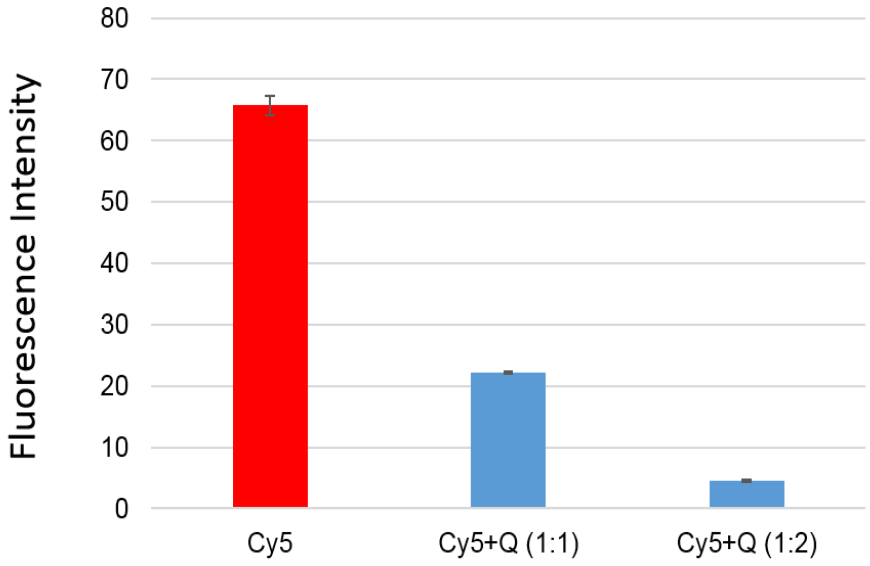

Figure 4.2 Fluorescence quenching experiment of the RNA splint with a Cy5 dye. “Cy5” represented the RNA splint with a Cy5 dye. “Cy5+Q” represented the mixture of the RNA splint and the DNA complementary splint.

Figure 4.2 shows the fluorescence signal from a mixture of the Cy5-labeled RNA splint and the DNA complementary splint conjugated with a quencher. With increasing concentration of the DNA complementary splint, the fluorescence signal from the RNA splint decreased dramatically, suggesting that the RNA splint stably base paired with the quencher-labeled DNA complementary splint. When the ratio of the RNA splint and DNA complementary splint went up to 1:2, the fluorescence signal decreased to approximately zero,

indicating that, at this point, the quencher completely suppressed the emission of the Cy5 dye.

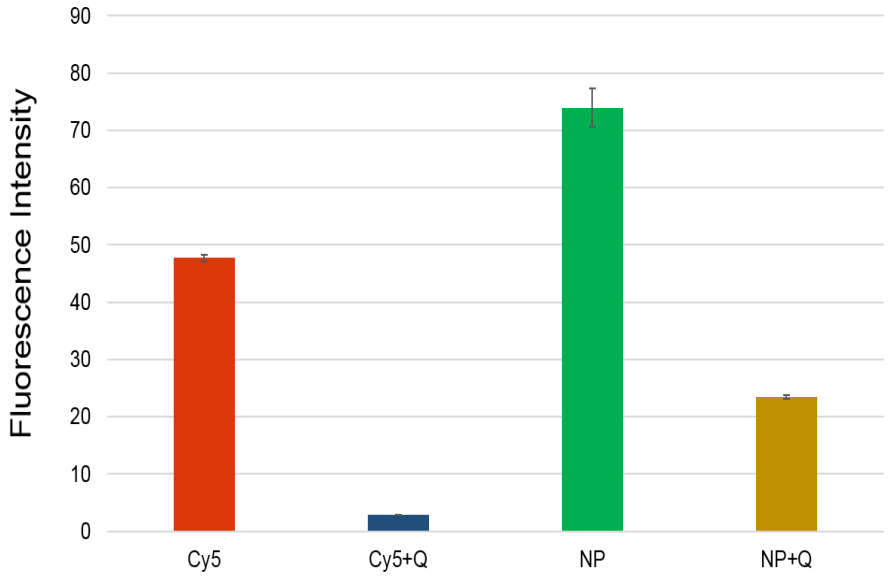

Figure 4.3 Fluorescence quenching experiment of the nanoprism containing the RNA splint with a Cy5 dye. “Cy5” represented the RNA splint with a Cy5 dye. “Cy5+Q” represented the mixture of the RNA splint and the DNA complementary splint. “NP” represented the sample containing the RNA splint and the two extended triangles. “NP+Q” represented the mixture including the RNA splint, DNA complementary splint and two extended triangles.

Figure 4.3 showed the result of the fluorescence quenching experiment of the nanoprism. A sample containing two extended triangles and the RNA splint (NP sample) exhibited a strong signal different from the signal exhibited by the RNA splint (Cy5) only, demonstrating that the RNA splint was incorporated in a different construct which was likely to be the nanoprism. This conclusion was further corroborated by comparing a sample containing the RNA splint and the DNA complementary splint (Cy5+Q) and a sample containing two extended triangles, the RNA splint and the DNA complementary splint (NP+Q). As shown in Figure 4.3, the former sample (Cy5+Q) showed nearly zero fluorescence

signal. After adding the triangle components for forming the nanoprism, the signal (NP+Q) increased to a relatively high level, suggesting that the RNA splint was incorporated in the nanoprism construct.

To sum up, although the initial FRET experiment failed to show the formation of the nanoprism because of the unexpected dimer hybridization by two DNA splints, the subsequent fluorescence quenching experiment clearly indicated that the RNA splints combined two extended triangles to form the nanoprism.

4.3 Materials and Methods

Materials:

FRET and fluorescence quenching experiments were conducted on a Spectra Max Gemini XS Spectrofluorometer device (Molecular Devices, Sunnyvale, CA).

All RNA and DNA splints were purchased from IDT, Inc.

DNA splint with Cy3: 5’ /Cy3/ GTG TGG ACA G 3’. DNA splint with Cy5: 5’ /Cy5/ GTG TGG ACA G 3’.

RNA splint with Cy5: 5’ /Cy5/ GUG UGG ACA G 3’.

DNA complementary splint: 5’ AAG TCC ACC A /BHQ_2/ 3’

Methods:

FRET experiments: all samples at 500mM concentration were prepared in buffer containing 20mM Mg^{2+} by heating to 65ºC for 5 minutes and then incubating at 37ºC for 10 minutes before cooling down to 5ºC. Then, all samples were diluted to 50mM in 10mM HEPES (4-(2-hydroxyethyl)-1-piperazineethanesulfonic acid) buffer, pH=7. Emission filters were set at 550 and 665 nm. The Cy3 label was excited at 520nm and transferred fluorescence was read as Cy5 emission at 670nm. The reading process was conducted at 25ºC.

Fluorescence quenching experiment: all samples were prepared by using the protocol described above. The Cy5 label was excited at 620nm and the emission of the Cy5 label was read at 670nm. Fluorescence reading process was conducted at 25ºC.

Chapter 5. Atomic Force Microscopy (AFM)

5.1 AFM Results

Atomic force microscopy is a high resolution microscopy which is capable to visualize particles within nanometers scale. To provide more information about the self-assembling RNA nanoprism, the prism prepared by the one-pot protocol was imaged by AFM, along with the original nanotriangle as a control. AFM images showed well-separated and randomly-distributed particles (Figure 5.1), but failed to resolve the shape of the nanotriangle and the nanoprism due to limitation of resolution. To the best of my knowledge, the smallest RNA nanoobject that had previously been successfully resolved by AFM was a nanotriangle containing 228 nucleotides which was about 3 times larger than the nanotriangle described here.

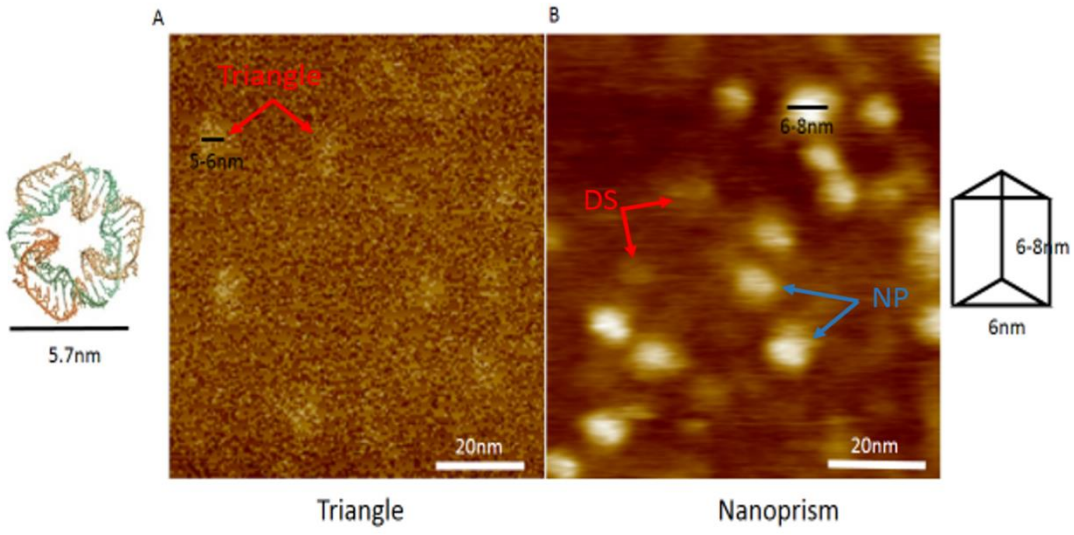

Figure 5.1 AFM images of the original nanotriangle (A) and the nanoprism (B).

AFM revealed the nanotriangle (Figure 5.1A) as a particle with average size of 5.5±0.5nm, which is in an excellent agreement with the size of the triangle observed in the x-ray crystal structure (5.7nm) (25). The nanoprism (NP) in the AFM images was slightly larger (6-8nm), which is consistent with the expected size, considering that deposition of the prism RNA on the mica surface likely leads to a partial collapse of the structure. It is worth noting that some dark spots (DS) in the nanoprism image might be indicative of by-products, such as single extended triangles not incorporated into prisms, which were also seen as satellite bands in the gel analyses.

Therefore, although AFM failed to resolve the shape of the nanoprism, randomly distributed particles of a homogeneous size indicated that a well-defined structure had been prepared and deposited on the AFM mica carrier. More importantly, AFM images clearly showed that a larger construct with the expected size of the nanoprism than the original nanotriangle was prepared. These AFM experiments provide further support for the formation of the designed RNA nanoprism.

5.2 Materials and Methods

Materials: The Atomic Force Microscope system used for the experiment was Bruker’s Dimension Icon. Access to the AFM instrument was kindly provided by the Gianneschi group.

Methods: 5µL RNA nanoprism and 5 µL RNA nanotriangle were prepared in solution before depositing on freshly cleaved mica surface. The nanoprism was prepared by using the one-pot protocol as described in Chapter 3, while the nanotriangle was prepared by following the protocol in a previous report (25). After waiting for 120 seconds, 2mM $Mg(OAc)_2$ buffer was used to wash the mica surface to remove other excess salt. Mica samples carrying RNA constructs were then air dried at room temperature. AFM images were taken in tapping/contact hybrid mode at room temperature and the images were processed with the Nanoscope Analysis Software.

Conclusions

In this study, I reported the design, construction and characterization of a triangular nanoprism made from fully double-stranded RNA. The nanoprism was prepared by extending a nanotriangle previously developed by our lab and then combining two extended triangles with DNA or RNA splints. The extension of the nanotriangle and the formation of the nanoprism were investigated by native polyacrylamide gel electrophoresis. Fluorescence quenching experiments further corroborated the interaction between the RNA splints and overhangs from the extended triangles. Although atomic force microscopy was not able to resolve the shape of the nanoprism due to the resolution limitation, discrete particles with the expected size of the nanoprism were seen clearly. The AFM results, in conjunction with the gel electrophoresis analyses and fluorescence quenching experiments, demonstrated the successful preparation of the designed three-dimensional RNA architecture.

Building a self-assembling, stable RNA nanostructure is a great challenge in the emerging field of RNA nanotechnology. This study proved the possibility to build a hierarchically assembled RNA object from an existing structure, which provides an attractive way to design and build three-dimensional RNA architectures with diverse shapes. To the best of my knowledge, this triangular nanoprism is the smallest circularly-closed three-dimensional nanoobject made of fully double-stranded RNA so far reported.

Reference

1. Crick F (1970) Central dogma of molecular biology. *Nature* 227(5258):561–563.

2. Egli M (2006) *“ DNA and RNA structure .”*

3. Alberts B (2002) *Molecular Biology of the Cell*.

4. Lund E, Dahlberg JE (2006) Substrate selectivity of exportin 5 and Dicer in the biogenesis of microRNAs. *Cold Spring Harb Symp Quant Biol* 71:59–66.

5. Brown CJ (1992) The human XIST gene: Analysis of a 17 kb inactive X-specific RNA that contains conserved repeats and is highly localized within the nucleus. *Cell* 71(3):527–542.

6. de V, JM N, Wachter D (1990) Small ribosomal subunit RNA sequences, evolutionary relationships among different life forms, and mitochondrial origins. 30:463–76.

7. Lagashetty A, Venkataraman A (2005) Polymer Nanocomposites. *Resonance* 10:49–57.

8. Ramos-De Valle LF (2013) Principles of Polymer Processing. *Handbook of Polymer Synthesis, Characterization, and Processing*, pp 451–461.

9. Sivertsen K (2007) Polymer foams. *3063 Polym Phys*:1–2

10. Li H (2015) RNA as a stable polymer to build controllable and defined nanostructures for material and biomedical applications. *Nano Today* 10(5):631–655.

11. Chworos A (2004) Building programmable jigsaw puzzles with RNA. *Science (80-)* 306(5704):2068–2072.

12. Jaeger L, Leontis NB (2000) Tecto-RNA: One-dimensional self-assembly through tertiary interactions. *Angew Chemie - Int Ed* 39(14):2521–2524.

13. Seeman NC (1982) Nucleic acid junctions and lattices. *J Theor Biol*

99(2):237–247.

14. Seeman NC (1998) DNA nanotechnology: novel DNA constructions. *Annu Rev Biophys Biomol Struct* 27:225–248.

15. Seeman NC (2007) An Overview of Structural DNA Nanotechnology. *Mol Biotechnol* 37(3):246–257.

16. Shih WM, Quispe JD, Joyce GF (2004) A 1.7-kilobase single-stranded DNA that folds into a nanoscale octahedron. *Nature* 427(6975):618–621.

17. Sugimoto N (1995) Thermodynamic Parameters To Predict Stability. *Biochemistry* 34:11211–11216.

18. Sugimoto N, Nakano SI, Yoneyama M, Honda KI (1996) Improved thermodynamic parameters and helix initiation factor to predict stability of DNA duplexes. *Nucleic Acids Res* 24(22):4501–4505.

19. Chang KY, Tinoco I (1994) Characterization of a “kissing” hairpin complex derived from the human immunodeficiency virus genome. *Proc Natl Acad Sci U S A* 91(18):8705–9.

20. Guo P (2005) RNA Nanotechnology: Engineering, Assembly and Applications in Detection, Gene Delivery and Therapy. *J Nanosci Nanotechnol* 5(12):1964–1982.

21. Guo P, Zhang C, Chen C, Garver K, Trottier M (1998) Inter-RNA interaction of phage phi29 pRNA to form a hexameric complex for viral DNA transportation. *Mol Cell* 2:149–155.

22. Shu D, Shu Y, Haque F, Abdelmawla S, Guo P (2011) Thermodynamically stable RNA three-way junction for constructing multifunctional nanoparticles for delivery of therapeutics. *Nat Nanotechnol* 6(10):658–667.

23. Haque F (2012) Ultrastable synergistic tetravalent RNA nanoparticles for targeting to cancers. *Nano Today* 7(4):245–257.

24. Shu D, Moll WD, Deng Z, Mao C, Guo P (2004) Bottom-up assembly of RNA arrays and superstructures as potential parts in nanotechnology. *Nano Lett* 4(9):1717–1723.

25. Boerneke MA, Dibrov SM, Hermann T (2016) Crystal-Structure-Guided Design of Self-Assembling RNA Nanotriangles. *Angew Chemie Int Ed*:n/a–n/a.

26. Dibrov SM, McLean J, Parsons J, Hermann T (2011) Self-assembling RNA square. *Proc Natl Acad Sci U S A* 108(16):6405–8.

27. Khisamutdinov EF (2014) Enhancing immunomodulation on innate immunity by shape transition among RNA triangle, square and pentagon nanovehicles. *Nucleic Acids Res* 42(15):9996–10004.

28. Severcan I (2010) A polyhedron made of tRNAs. *Nat Chem* 2(9):772–779.

29. Yu J, Liu Z, Jiang W, Wang G, Mao C (2015) De novo design of an RNA tile that self-assembles into a homo-octameric nanoprism. *Nat Commun* 6:5724.

30. Aldaye F a, Palmer AL, Sleiman HF (2008) Assembling materials with DNA as the guide. *Science* 321(5897):1795–1799.

31. Seeman NC (2010) Nanomaterials based on DNA. *Annu Rev Biochem* 79:65–87.

32. Zhang F, Nangreave J, Liu Y, Yan H (2014) Structural DNA nanotechnology: State of the art and future perspective. *J Am Chem Soc* 136(32):11198–11211.

33. Geary C, Rothemund PWK, Andersen ES (2014) A single-stranded architecture for cotranscriptional folding of RNA nanostructures. *Science (80-)* 345(6198):799–804.

34. Endo M, Takeuchi Y, Emura T, Hidaka K, Sugiyama H (2014) Preparation of chemically modified RNA origami nanostructures. *Chemistry* 20(47):15330–15333.

35. Loening UE (1967) The fractionation of high-molecular-weight ribonucleic acid by polyacrylamide-gel electrophoresis. *Biochem J* 102:251–257.

36. Bio-Rad (2014) A Guide to Polyacrylamide Gel Electrophoresis and Detection. *Bio-Rad*:92.

37. Westermeier R (2005) Gel Electrophoresis. *Encyclopedia of Life Sciences*, pp 1–6.

38. Lord M (2003) Gel Electrophoresis of Proteins. *Essent Cell Biol*:197–268.

39. B.D H (2013) *Gel Elektrophoresis of Proteins A Practical Approach* (OXFORD UNIVERSITY PRESS) doi:10.1017/CBO9781107415324.004.

40. Priyakumar UD, Hyeon C, Thirumalai D, MacKerell AD (2009) Urea destabilizes RNA by forming stacking interactions and multiple hydrogen bonds with nucleic acid bases. *J Am Chem Soc* 131(49):17759–17761.

41. Förster T (1960) Transfer mechanisms of electronic excitation energy. *Radiat Res Suppl* (10):7–17.

42. Hildebrandt N (2014) How to Apply FRET: From Experimental Design to Data Analysis. *… Energy Transf From Theory to Appl*. doi:10.1002/9783527656028.

43. Kim HD (2002) Mg2+-dependent conformational change of RNA studied by fluorescence correlation and FRET on immobilized single molecules. *Proc Natl Acad Sci U S A* 99(7):4284–9.

44. Schaufele F (2005) The structural basis of androgen receptor activation: intramolecular and intermolecular amino-carboxy interactions. *Proc Natl Acad Sci U S A* 102(28):9802–7.

45. Zhuang X (2000) A single-molecule study of RNA catalysis and folding. *Science* 288(5473):2048–2051.

46. Lipman E a, Schuler B, Bakajin O, Eaton W a (2003) Single-molecule measurement of protein folding kinetics. *Science* 301(5637):1233–1235.

47. Kretschy N, Sack M, Somoza MM (2016) Sequence-Dependent Fluorescence of Cy3- and Cy5-Labeled Double-Stranded DNA. *Bioconjug Chem*:acs.bioconjchem.6b00053.

48. Conley NR, Biteen JS, Moerner WE (2008) Cy3-Cy5 covalent heterodimers for single-molecule photoswitching. *J Phys Chem B* 112(38):11878–11880.

49. Pawley JB (1996) Handbook of Biological Confocal Microscopy, Second Edition. *Opt Eng* 35(9):2765.

50. Peng X, Draney DR, Volcheck WM (2006) Quenched near-infrared fluorescent peptide substrate for HIV-1 protease assay. *Proc SPIE* 6097:60970F–60970F–12.

51. Zadran S (2012) Fluorescence resonance energy transfer (FRET)-based biosensors: Visualizing cellular dynamics and bioenergetics. *Appl Microbiol Biotechnol* 96(4):895–902.

52. Kreder R (2015) Solvatochromic Nile Red Probes with FRET Quencher Reveal Lipid Order Heterogeneity in Living and Apoptotic Cells. *ACS Chem Biol*:150306062704000.

53. Binnig G, Quate CF (1986) Atomic Force Microscope. *Phys Rev Lett* 56(9):930–933.

54. Cappella B, Dietler G (1999) Force-distance curves by atomic force microscopy. *Surf Sci Rep* 34(1-3):1–104.

55. Bustamante C (1992) Circular DNA molecules imaged in air by scanning force microscopy. *Biochemistry* 31(1):22–26.

56. Liu Z (2005) Observation of the mica surface by atomic force microscopy. *Micron* 36(6):525–531.

57. Shlyakhtenko LS (2003) Silatrane-based surface chemistry for immobilization of DNA, protein-DNA complexes and other biological materials. *Ultramicroscopy* 97(1-4):279–287.

58. Lyubchenko YL, Shlyakhtenko LS, Ando T (2011) Imaging of nucleic acids with atomic force microscopy. *Methods* 54(2):274–283.

59. Yan H, Park SH, Finkelstein G, Reif JH, LaBean TH (2003) DNA-templated self-assembly of protein arrays and highly conductive nanowires. *Science* 301(5641):1882–1884.

60. Yan H, LaBean TH, Feng L, Reif JH (2003) Directed nucleation assembly of DNA tile complexes for barcode-patterned lattices. *Proc Natl Acad Sci U S A* 100(14):8103–8108.

61. Yodh JG, Woodbury N, Shlyakhtenko LS, Lyubchenko YL, Lohr D (2002) Mapping nucleosome locations on the 208-12 by AFM provides clear evidence for cooperativity in array occupation. *Biochemistry* 41(11):3565–3574.

62. Hizume K (2002) Chromatin reconstitution: development of a salt-dialysis method monitored by nano-technology. *Arch Histol Cytol* 65(5):405–413.

63. Zhong, Q., Innis, D., Kjoller, K., Elings VB, Zhong Q, Inniss D, Kjoller K, Elings VB (1993) Fractured polymer/silica fiber surface studied by tapping mode atomic force microscopy. *Surf Sci Lett* 290(1-2):L688–L692.

64. Magonov SN, Elings V, Whangbo M-H (1997) Phase imaging and stiffness in tapping-mode atomic force microscopy. *Surf Sci* 375(2-3):L385–L391.

65. Geisse NA (2009) AFM and combined optical techniques. *Mater Today* 12(7-8):40–45.

66. Oussatcheva E (1999) Structure of branched DNA molecules: gel retardation and atomic force microscopy studies. *J Mol Biol* 292(1):75–86.

67. Grzybowski B (2014) tures lack the structural resolution and diversity of RNA tertiary motifs (22), such as kissing-loop. 2421(2002):2418–2421.

68. Nudler E, Mironov AS (2004) The riboswitch control of bacterial metabolism. *Trends Biochem Sci* 29(1):11–17.

69. Tucker BJ, Breaker RR (2005) Riboswitches as versatile gene control elements. *Curr Opin Struct Biol* 15(3 SPEC. ISS.):342–348.

70. Dibrov SM (2012) Structure of a hepatitis C virus RNA domain in complex with a translation inhibitor reveals a binding mode reminiscent of riboswitches. *Proc Natl Acad Sci* 109(14):5223–5228.

71. Dibrov SM, Johnston-Cox H, Weng YH, Hermann T (2007) Functional architecture of HCV IRES domain II stabilized by divalent metal ions in the crystal and in solution. *Angew Chemie - Int Ed* 46(1-2):226–229.

72. Boerneke MA, Dibrov SM, Gu J, Wyles DL, Hermann T (2014) Functional conservation despite structural divergence in ligand-responsive RNA switches. *Proc Natl Acad Sci U S A* 111(45):15952–7.

73. Wang Y (2008) C3-Spacer-containing circular oligonucleotides as inhibitors of human topoisomerase I. *Bioorganic Med Chem Lett* 18(12):3597–3602.

74. Sato Y (2009) Influence of substituent modifications on the binding of 2-amino-1,8-naphthyridines to cytosine opposite an AP site in DNA duplexes: Thermodynamic characterization. *Nucleic Acids Res* 37(5):1411–1422.

75. Salazar M, Fedoroff O, Miller JM, Ribeiro NS, Reid B (1993) The DNA strand in DNA.RNA hybrid duplexes is neither B-form nor A-form in solution. *Biochemistry* 32(16):4207–15.